Nanoscale

Chemical Potential Gradient Induced Formation of Kirkendall Voids at Epitaxial TiN/MgO Interface

Journal:	*Nanoscale*
Manuscript ID	NR-ART-04-2023-001860.R2
Article Type:	Paper
Date Submitted by the Author:	18-Jul-2023

Complete List of Authors:	Zhang, Xiaoman; Louisiana State University, Mechanical and Industrial Engineering Department Meng, Wen; Louisiana State University, Mechanical and Industrial Engineering Department Meng, Andrew; University of Missouri, Physics and Astronomy

SCHOLARONE™
Manuscripts

Please do not adjust margins

ARTICLE

Received 00th January 20xx,
Accepted 00th January 20xx
DOI: 10.1039/x0xx00000x

Chemical Potential Gradient Induced Formation of Kirkendall Voids at Epitaxial TiN/MgO Interface

Xiaoman Zhang,[1] W. J. Meng,[1] Andrew C. Meng[2]

We report the observation of Kirkendall voids at the epitaxial titanium nitride (TiN)/magnesium oxide(MgO)(001) interface. While epitaxial growth of TiN on MgO has been known for years, many reports show a perfectly sharp epitaxial interface. Because TiN is a prototypical diffusion barrier material, observing the consequence of rapid diffusion at a TiN interface is interesting. Structural characterization of the interface using x-ray diffraction and electron microscopy confirms the diffuse nature of the interface. Rectangular voids that form at the TiN/MgO(001) interface and extend into both TiN and MgO result from a large chemical potential gradient at the interface, which contributes a strong chemical driving force for diffusion. The spatial localization of the observed voids is limited to within ~10 nm from the interface, consistent with a chemical potential gradient driving force. A composition gradient on the nanometer scale is also observed. Observation of Kirkendall voids at this nitride/oxide interface suggests possibilities for engineering oxygen and nitrogen vacancies at thin film interfaces.

Introduction

Nitride/oxide interfaces have been studied for many applications in electronics. Their chemistry is relevant to wide ranging materials systems from oxide gate dielectrics on nitride semiconductors,[1-6] oxynitride gate dielectrics on silicon and germanium,[7, 8] and nanowire heterostructures.[9-11] There have been many recent studies on interfaces between titanium nitride and oxides due to the widespread use of titanium nitride (TiN) as a bottom electrode for metal/oxide/metal functional devices for resistive[12, 13] and ferroelectric[1-3] random access memory applications. Some device performance improvements are attributed to the presence of TiN, and there are studies focusing on structural characterization that suggest that TiN plays a role in crystallization of and ferroelectric behavior of hafnium oxide films,[2, 4, 14] and can influence crystallographic texture.[5] The strong influence of vacancies on the electrical properties of many functional oxides[15-17] means that an understanding of vacancy behavior at nitride/oxide interfaces may prove useful for tunable control over functional properties, particular when the oxide film is very thin such as in highly scaled random-access memory devices.[18, 19] Here, we study TiN thin films grown epitaxially on magnesium oxide (MgO) substrates as a controlled model system to examine the influence of chemical driving forces at the interface.

[a] Department of Mechanical and Industrial Engineering, Louisiana State University, Baton Rouge, LA 70803
[b] Department of Physics and Astronomy, University of Missouri, Columbia, MO 65211
† Footnotes relating to the title and/or authors should appear here.
Electronic Supplementary Information (ESI) available: [details of any supplementary information available should be included here]. See DOI: 10.1039/x0xx00000x

The TiN/MgO system has been studied since the 1980s,[20, 21] and it is well known that TiN can be epitaxially grown using reactive sputtering.[22, 23] TiN and MgO are isostructural, both having the halite structure, and have a bulk lattice mismatch of less than 1%.[24] There are combined experiment and simulation studies consistent with cation-anion bonding (e.g. Ti-O and Mg-N) at the interface,[25, 26] and solid-state interfacial reactions for formation of the spinel phase or other compounds are known.[27-29] Thus, the chemical interaction between the nitride and oxide is non-negligible. Oxygen contamination in TiN is well-known,[30] and Ti is also known to form oxynitrides,[31, 32] so there are potentially other competing interfacial processes as well. On the other hand, there are many reports arguing that the epitaxial TiN/MgO interface is sharp, as evidenced by Scanning/Transmission Electron Microscope (S/TEM) imaging at atomic resolution in films grown by both pulsed laser deposition and reactive sputtering and for growth temperatures as high as 800 °C.[33-35] Such reports imply that interactions between TiN and MgO do not interfere with binding sufficiently to cause significant atom migration. This apparent paradox could be rationalized in several ways: 1) growth conditions can be varied to limit the kinetic processes related to diffusional mixing at the interface; 2) differences in as-grown vacancy concentrations could influence chemical potential gradient induced diffusion at the interface; 3) the appearance of sharp contrast at an interface in TEM or STEM images does not guarantee that the interfacial composition profile is atomically sharp.

Here, we report epitaxial growth of TiN films on MgO (001) using reactive sputtering. Epitaxy is confirmed through X-ray diffraction (XRD). Structural characterization of the interface is performed using TEM, STEM, and energy dispersive X-ray spectroscopy (EDS) compositional mapping. Although upon first

Please do not adjust margins

observation, many regions of the interface appear perfectly sharp through imaging techniques, we observe regularly spaced rectangular Kirkendall voids in as-grown TiN/MgO(001) specimens that extend from the TiN film into the MgO substrate. This observation and the observation of a graded interfacial composition profile are consistent with atom migration due to imbalanced diffusion during growth. The atom migration process at the interface could potentially be used to intentionally generate vacancies at nitride-oxide interfaces in an epitaxial multilayer structure. It is also important to note that interactions at the heteroepitaxial interface not only include chemical driving forces for diffusion, but also misfit strain.

Experimental

TiN films were deposited using reactive magnetron sputtering in a custom-built ultra-high-vacuum (UHV) system with a base pressure below 5 × 10^{-10} Torr. The growth chamber, which is pumped by a turbomolecular pump (Pfeiffer HiPace 800) and a cryogenic pump (Marathon® CP-8), is connected to a load-lock that is also pumped by a turbomolecular pump (Pfeiffer HiPace 300). MgO(001) substrates were purchased from the MTI Corporation, degreased in acetone and ethanol, and finally cleaned by annealing in the growth chamber prior to growth. Si targets (75mm diameter, 99.95 at%) and Ti targets (75 mm diameter, 99.95 at%) are used. During TiN film growth, the MgO substrate was heated radiatively from the back side using a SiC electric heater. Because the MgO substrate is transparent, a Si film was deposited separately at room temperature onto its back side to act as a heat susceptor prior to it being loaded into the growth chamber. The temperature of a separate Si substrate was measured using direct optical access infrared pyrometry, with the emissivity of Si set at 0.68. The temperature was simultaneously read from a thermocouple placed in close proximity of the substrate, and the calibrated thermocouple reading was subsequently used to indicate the substrate temperature during actual growth runs. Growths were carried out at ~850°C in an Ar/N_2 mixture with a total pressure of ~4.5 mTorr, with two Ti targets operated in the dc mode at 1.65 A. The gas input flow rates were 20.0 and 6.5 sccm for Ar (99.999%+) and N_2 (99.999%+), respectively. A substrate bias of -40 V was used. After growth, specimens were cooled to room temperature before being transferred out of the growth system.

X-ray diffraction (XRD) data were collected on a PANalytical Empyrean instrument using monochromated Cu $K\alpha_1$ radiation via a 2 crystal Ge(220) 4-bounce monochromator. Samples were mounted on a χ-ϕ-x-y-z stage, allowing symmetric $\theta/2\theta$, asymmetric ϕ, and ω rocking curve scans to be performed. Scan rates of 0.18 deg/s, 1 deg/s, and 0.5 deg/s, and scan steps of 0.05 deg, 1 deg, and 0.01 deg, were used for $\theta/2\theta$, ϕ, and ω scans, respectively. Scattered x-rays were collected using a PIXcel 3D detector. Transmission electron microscopy (TEM) samples were prepared using a ThermoFisher Helios G4 Xe^+ plasma focused ion beam/scanning electron microscope (PFIB/SEM). Electron beam induced deposition of Pt, followed by ion beam induced deposition of Pt was used to protect the sample from the ion beam. The sample was thinned at successively lower accelerating voltages, with final thinning performed at 2 kV. S/TEM experiments were performed in a double aberration corrected ThermoFisher Spectra 300 S/TEM instrument. HAADF STEM images were acquired with 21 mrad convergence angle and 32 pA probe current. The microscope is equipped with Super-X silicon drift detectors (SDD) for EDS with 0.7 sr solid angle. For acquisition of drift-corrected STEM-EDS maps, 80 pA probe current was used. Integrated differential phase contrast (iDPC) STEM images were collected using a segmented STEM detector.

Results and Discussion

To confirm the epitaxial relationship between the TiN film and the MgO substrate, XRD is used. Figure 1a shows a typical $\theta/2\theta$ symmetric scan. In addition to the (002) family of MgO substrate peaks, all TiN reflections can be indexed to those of the (002) family. The off-axis asymmetric ϕ-scans shown in Fig. 1b show that the (204) reflections of the TiN film are aligned with the (204) reflections of the MgO substrate. The ω rocking curves, shown in Figure 1c, indicate a full-width-at-half-maximum (FWHM) of 0.05° for the MgO substrate and 0.11° for the TiN film. The data shown in Fig. 1 indicate that the TiN film is grown epitaxially on the MgO(001) substrate with a cube-on-cube orientation relationship, with TiN (001) ‖ MgO (001) out-of-plane and TiN [100] ‖ MgO [100] in-plane.

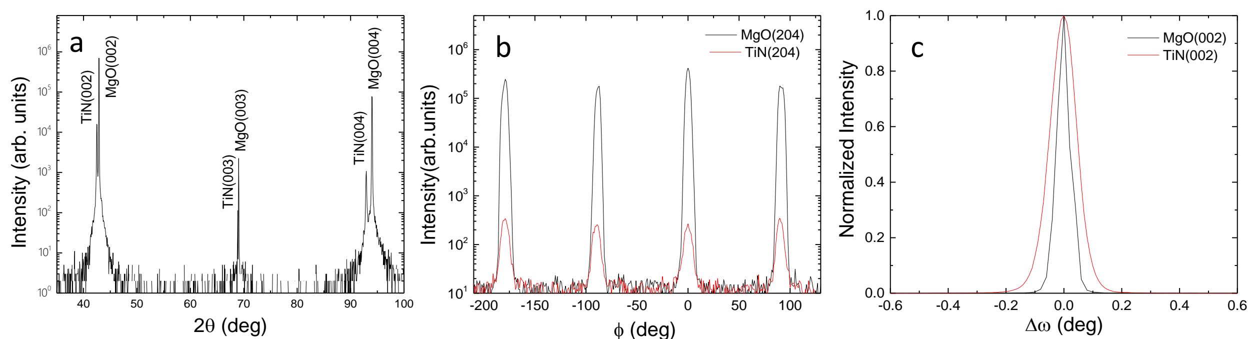

Figure 1. XRD (a) θ-2θ scan, (b) off-axis asymmetric ϕ-scan, and (c) ω-scan of one TiN thin film grown on a MgO (001) substrate.

This journal is © The Royal Society of Chemistry 20xx

Please do not adjust margins

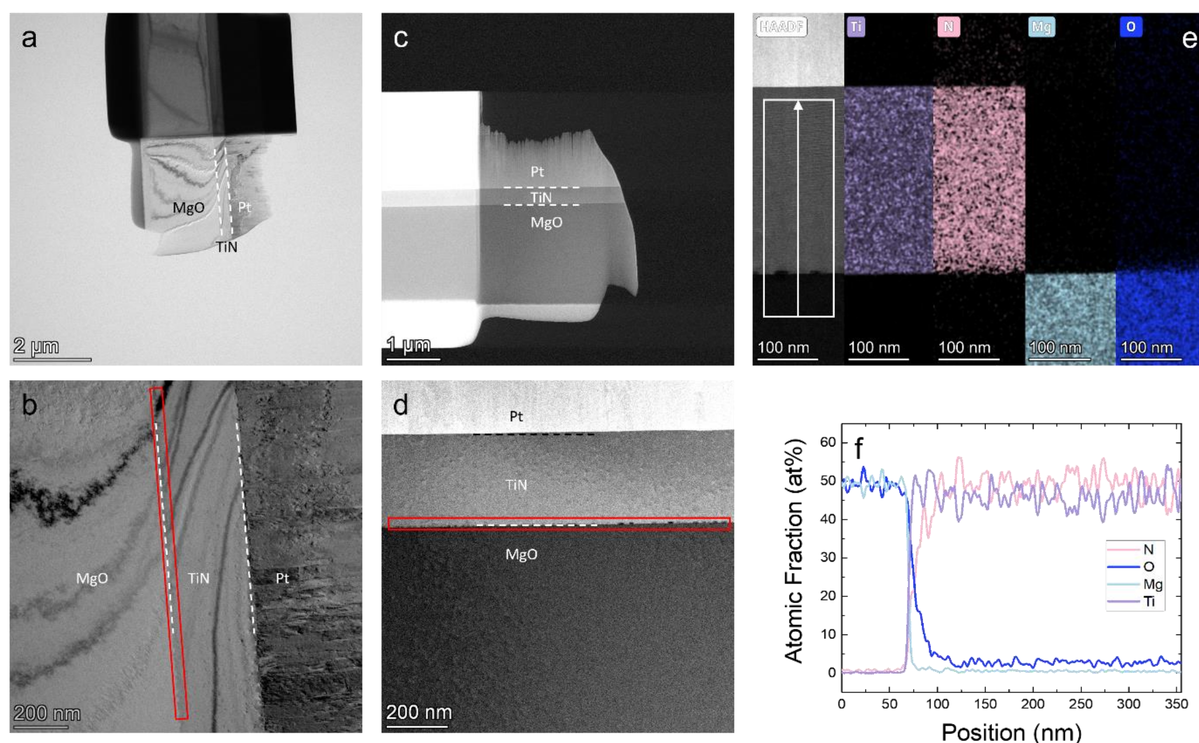

Figure 2. Low magnification cross-sectional TEM (a-b) images, STEM(c-d) images, and STEM EDS (e) maps and (f) line scan. The red regions of interest highlight rectangular regions of brighter contrast in TEM (b) and darker contrast in STEM (d).

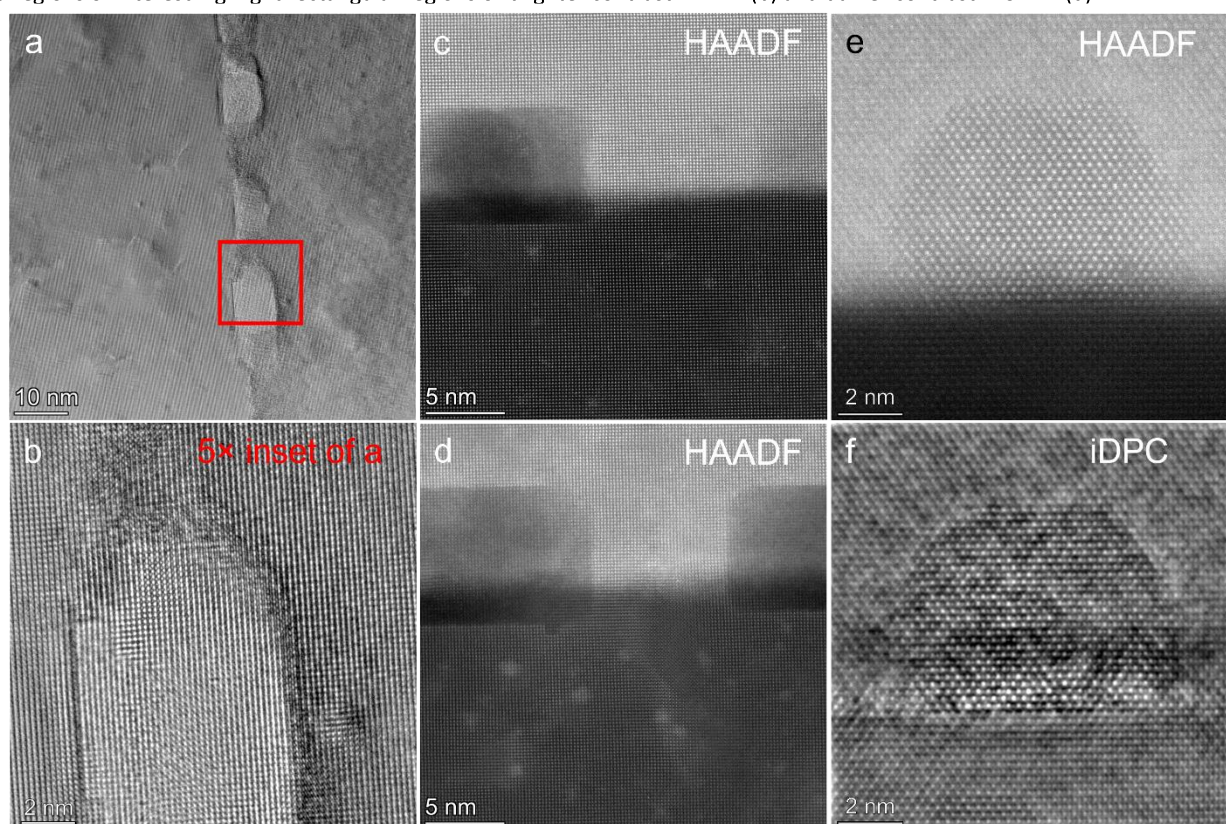

Figure 3. (a) A HRTEM image of the TiN/MgO (001) interface; (b) 5× Inset of a); (c/d) HAADF STEM images of the TiN/MgO(001) interface; the small trapezoidal region with a darker contrast in STEM is consistent with a void in both the (e) HAADF STEM image and the (f) iDPC STEM image.

The structure of the epitaxial TiN/MgO (001) interface is first characterized using TEM and STEM imaging. At low magnification, the substrate and the film are easily distinguished in both the TEM image (Fig. 2a) and the high angle

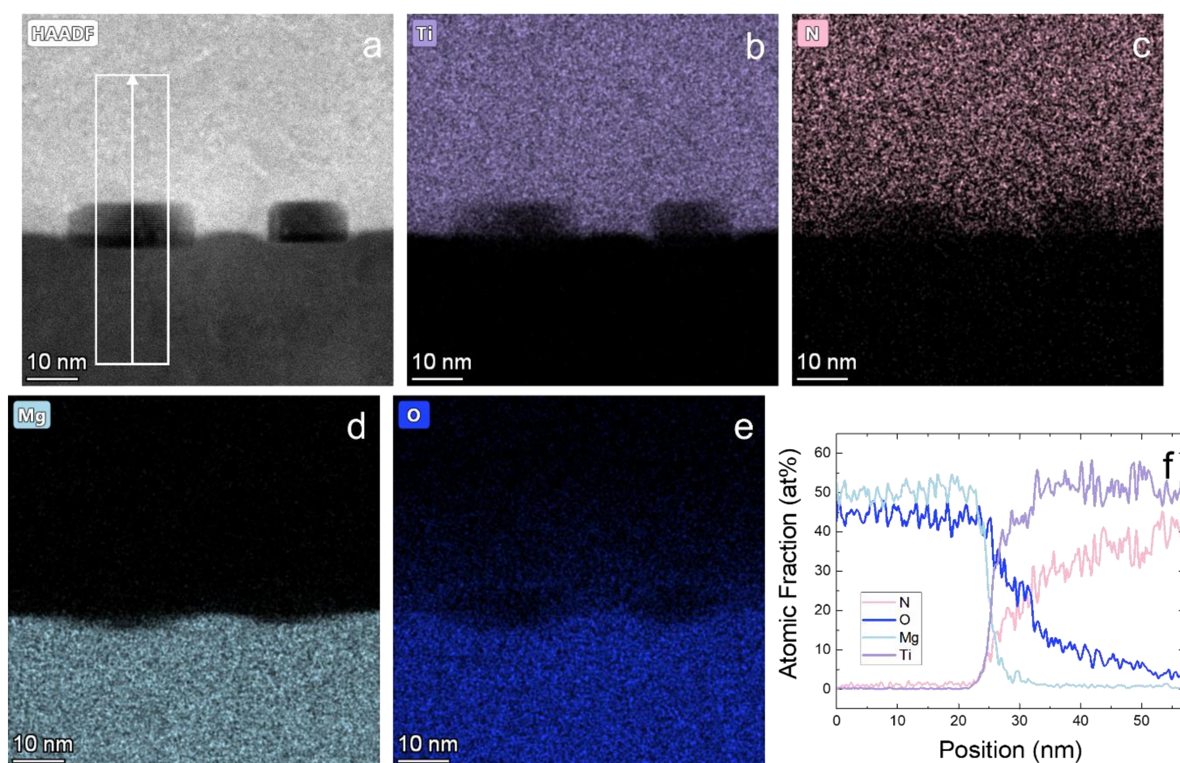

Figure 4. (a) HAADF STEM image of voids at the TiN/MgO (001) interface, and EDS maps for (b) Ti, (c) N, (d) Mg, (e) O signals, and (f) STEM EDS line scan through void region.

annular dark field (HAADF) STEM image (Fig. 2c). At low magnification, the TEM image (Fig. 2a) shows bend contour diffraction contrast and the HAADF STEM image (Fig. 2c) is relatively featureless. As the films are grown at 850°C under low substrate bias (-40V), the contrast in the low magnification TEM and STEM images indicates that polyhedral nitrogen bubbles typically observed in sputtered TiN films under high substrate bias (< -300 V) and low temperatures below 800°C are not observed, consistent with previous reports that such bubbles do not form for growth temperatures of 800°C and higher.[36] At higher magnification, small rectangles are observed at the TiN/MgO interface in both the TEM image (Fig. 2b) and HAADF STEM image (Fig. 2d). In the TEM image, these rectangles have a brighter contrast, while in the HAADF STEM image, they have a darker contrast. Diffraction contrast in the TEM image indicates that fewer electrons are scattered in these rectangular regions; mass-thickness contrast in the HAADF STEM image indicates that there is less material in these rectangular regions. Both imaging modes indicate consistently that these rectangular regions have less material than their surrounding regions.

Aberration corrected high resolution TEM (HRTEM) and aberration corrected STEM imaging is used to characterize the TiN/MgO(001) interface at the atomic scale. The rectangular regions span the TiN/MgO interface with one surface in TiN and the diametrically opposed surface in MgO (Fig. 3). Phase contrast shows continuous lattice fringes throughout the rectangular regions (Figs. 3a, 3b), consistent with the observation of atomic columns in the HAADF STEM images (Figs. 3c, 3d). The lattice fringes in the rectangular regions are slightly brighter than those in the surrounding areas (Figs. 3a, 3b). In the HAADF STEM images, the atomic columns are darker in the rectangular regions than in the surrounding areas (Figs. 3c, 3d). Such contrast is consistent with the observations at low magnification (Fig. 2). An integrated differential phase contrast (iDPC) STEM image (Fig. 3f) shows improved contrast from low atomic number elements such as oxygen and nitrogen by using a segmented dark field detector. Focusing on a region with reduced mass thickness at the interface (Fig. 3e), iDPC imaging observes that the region consists of faceted triangular subregions. In comparison, this contrast is not visible in the HAADF STEM image of the same region (Fig. 3e).

Elemental composition mapping is performed using STEM-EDS (Fig. 4 a-f). Here we note that the region in Fig. 4 is not the same as the one in Fig. 3. On the 10 nm scale, the interface is not sharp: oxygen signal in the TiN film is consistent with some diffusive mixing. The rectangular region shows a significantly lower count of characteristic X-rays, consistent with a decreased amount of material due to a void. A line-scan of the region in Fig. 4a is given in Fig. 4f and shows compositional grading at the interface consistent with interdiffusion. At the atomic scale, an EDS map of a region of the interface without a void shows significant compositional grading on the nm scale (Fig. 5). Ti and Mg compositions vary significantly over an approximately 1 nm distance, while N and O compositions vary over a significantly larger distance. The composition in the TiN region ~4.5 nm away from the interface is approximately 50 at% Ti, 20 at% N, and 20 at% O (bal. Mg). Similarly, the composition in the MgO region ~4 nm away from the interface is approximately 50 at% Mg, 40 at% O, and 5 at% N (bal. Ti) (Fig. 5b). While atomic columns are visible in the Ti and Mg EDS maps (Figs. 5c and 5e), they are not in the N and O EDS maps (Figs. 5d and 5f). There are two factors that contribute to this: first, lower Z elements generate fewer x-rays, resulting in a smaller signal

This journal is © The Royal Society of Chemistry 20xx

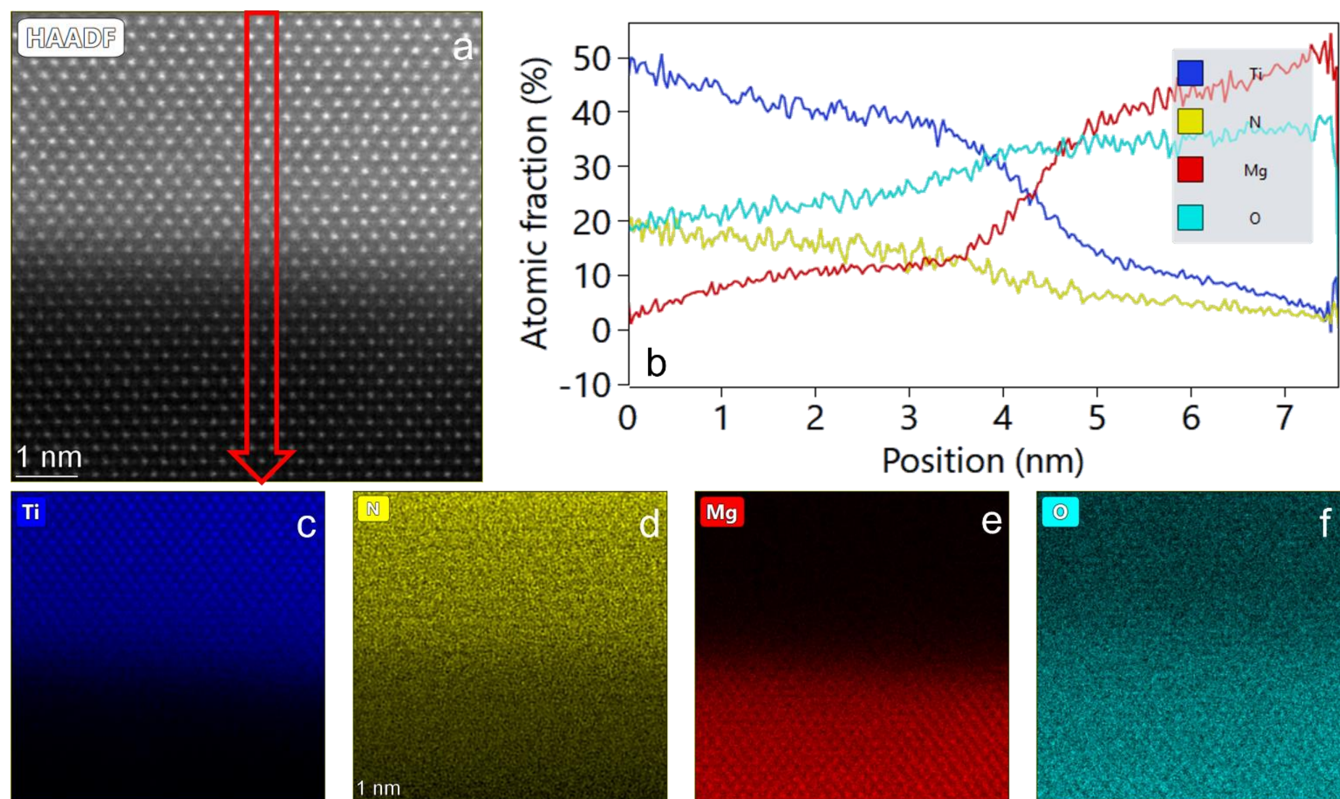

Figure 5. (a) A HAADF STEM image of the TiN/MgO interface, (b) atomic resolution STEM EDS line scan at TiN/MgO interface and EDS maps for c) Ti, d) N, e) Mg, and f) O signals

to noise ratio in the EDS data; second, N and O likely diffuse faster than Ti and Mg, resulting in more disorder in the anion sublattice.

Electrical properties of an epitaxial TiN film were measured using the Transmission Line Model method, and the results are shown in Fig. 6.[37, 38] Using contact spacings of 2 mm, 4 mm, and 6 mm, resistances of 8.09Ω, 8.90Ω, and 10.06Ω are measured, respectively (Fig. 6b) using Rh probes (250 µm diameter, Nextron Corp.). Fitting the contact resistance (Fig. 6c) and using the formula for the conductivity between two circular contacts at the rim of a disk[39] yields a resistivity of 53.7 µΩ cm for the TiN film. The result is on the low side of reported resistivities of sputtered TiN as-grown, which range from 30 µΩ cm to 170 µΩ cm.[40, 41]

While there are reports of polyhedral gas bubble precipitates in sputtered TiN films throughout the bulk film,[36] these are only observed under high substrate bias (V_s < -300V) for growth temperatures less than 800°C. As the growths for the current work are conducted at higher temperatures under lower substrate bias (-40V), it is likely that a different mechanism dominates. Another proposed mechanism is that polyhedral voids can be attributed to low adatom mobility conditions that promote atomic self-shadowing; this has been observed in TiN/NbN superlattice structures.[42] The present results, combined, show clear evidence of rectangular voids at the epitaxial TiN/MgO (001) interface. Coupled with the observation of a diffuse interface, this is consistent with imbalanced diffusion between TiN and MgO during growth. As TiN is a well-known diffusion barrier and MgO is a refractory

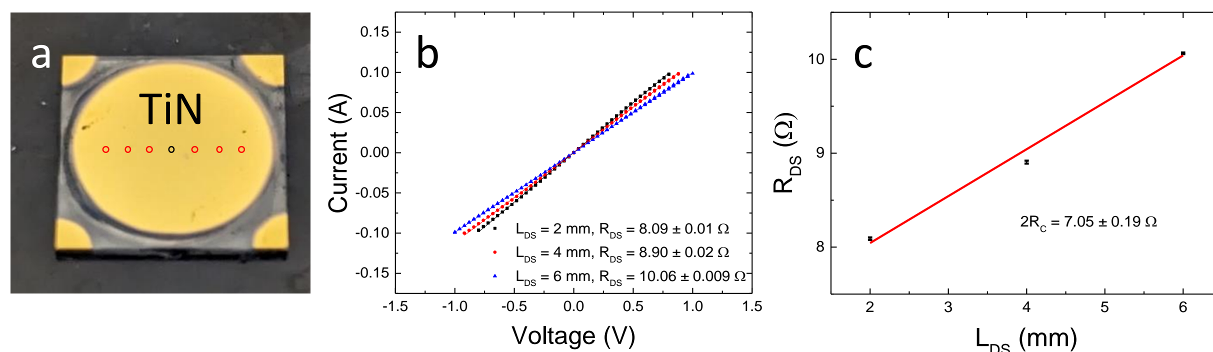

Figure 6. (a) Epitaxial TiN film on Mg (001): red circles indicate electrical contact positions, black circle indicates the center of the sample. Transmission line model (b) current-voltage characteristics as a function of contact spacing and (c) contact resistance fitting

ceramic, this may seem somewhat surprising. To rationalize the present observation, consider that the driving force for diffusion is a chemical potential gradient. Simulations consistent with Ti-O and Mg-N bonding at the interface[25, 26] then suggest that differences in Ti-O and Ti-N or Mg-O and Mg-N bond enthalpies could potentially lead to enthalpy of mixing interactions that influence chemical interdiffusion. Likely there are a combination of effects including modulations in surface adatom mobility and imbalanced diffusion at the interface that result in voids at the TiN/MgO interface. While diffuse composition changes at the interface are consistent with imbalanced diffusion, rectangular faceted voids suggest concurrent nucleation and growth of vacancy clusters at the interface that is influenced by anisotropy. On the other hand, we note that Kirkendall voids at epitaxial interfaces have been observed in a number of different material systems, including Cu(In,Ga)Se_2/GaAs,[43] $CaSi_2$/Si,[44] and ZnO/Si.[45]

Alternatively, considering that the microscopic mechanism(s) for atom migration in the TiN-MgO system is likely vacancy mediated, asymmetries in vacancy migration at or across the interface will generate imbalanced atom fluxes that will lead to the formation of Kirkendall voids. As a larger volume fraction of the voids is located in the TiN film side as compared to the MgO substrate side, the present data indicate a positive vacancy flux from the MgO substrate side towards the TiN film side. Conservation of lattice sites indicates that atomic flux from the TiN film side towards the MgO substrate side is greater than that from the substrate towards the film. In the literature, formation of Kirkendall voids during TiO_2 nanorod nitridation into oxynitride is known.[46] At the interface between TiO_2 and $TiN_{1-x}O_x$, the atomic flux points from the nitrogen rich region towards the oxide, consistent with an O diffusion rate that is greater than that of N. Our data shows the opposite—atomic flux points from the oxide towards the nitride. There are two possibilities, 1) the relative rates of O and N diffusion in the TiN/MgO system are reversed compared to that in the $TiN_{1-x}O_x/TiO_2$ system, or 2) the Mg diffusion rate is greater than that of Ti in the TiN/MgO system and this difference dominates the behavior at the interface. A combination of these effects is also possible. The second possibility is supported by the present STEM-EDS data: the Mg and Ti concentration profiles in Fig. 5b show that the Ti concentration decays slightly more (~ 50 at% to ~23 at%) than the Mg composition increases (~0 at% to 18 at%) over a distance of 4 nm. This distance, while arbitrary, was chosen so that the region of interest falls almost entirely in the TiN film in order to avoid complications from differences in diffusivity in TiN and MgO. Here, noting that MgO and TiN are ionic and mixed ionic/covalent compounds, the small ionic radius of Mg compared to the atomic radius of Ti is consistent with the observation of faster diffusion of Mg compared to Ti.

One subtlety is that it is likely more difficult to increase the void concentration at the interface than it is to decrease it because low growth temperatures in combination with low substrate bias limit both diffusion and gas bubble formation.[36] There are previous reports of spinel formation at the TiN/MgO interface when the growth temperature is greater than 800 °C or when specimens are post-annealed at 850 °C.[28, 36] Interestingly, no spinel formation is observed as might be expected for the growth temperature (850 °C), even though no post-growth anneal is performed. As spinel formation depends on the kinetics of the solid-state reaction, the shorter growth duration needed for the low thickness of the present TiN film (~300 nm) as compared to that for the previous reports (for growing a ~2 µm thick TiN film)[36] where spinel formation was observed may be in part responsible for this difference. At high growth temperature and low substrate bias, vacancy diffusion kinetics driven by the sharp chemical potential gradient at the interface control dynamics of void formation. To avoid void formation, low growth temperature and low substrate bias may be used.[36]

Nitrogen and oxygen vacancies play an important role in electrical conductivity of nitrides[47] and oxides,[48] respectively. For optoelectronic devices with nitride or oxide active materials, controlling vacancies at the nitride-oxide interface could potentially be used to tune device behavior. For example, vacancies could be intentionally clustered at an interface in a multilayer structure to generate a 2D layer with vacancies acting as charge carriers analogous to a 2D electron gas. Separately, nitride-oxide interfaces could be designed through doping to minimize chemical interaction induced void formation either by reducing the magnitude of the enthalpy of mixing or by balancing diffusion of atoms across the interface to prevent vacancy buildup. This could be important in reducing defects in heteroepitaxial nitride films where crystallographic defects arising from the foreign substrate can have deleterious effects for functional behavior.

Conclusions

We report combined structural characterization from XRD, TEM, and STEM-EDS of epitaxial TiN films on MgO (001) substrates grown by reactive dc magnetron sputtering. Characterization of the TiN/MgO (001) interface indicates the presence of nanoscale, rectangular Kirkendall voids. While this material system has been well-studied since the 1980s, and interfacial reactions at the interface of epitaxial TiN films on MgO are known, our observations of void formation consistent with chemically driven imbalanced diffusion suggest the potential to tune electrical properties of, for example, functional oxide semiconductors, grown on TiN electrodes by modulating vacancy concentration. While investigation of the dynamics of the epitaxial interface under growth conditions using in-situ TEM could prove promising, there are significant challenges to replicating high temperature sputter deposition conditions in existing commercial TEM gas cells. The observation of Kirkendall voids despite TiN being a prototypical diffusion barrier material reinforce the strong chemical nature of the driving force at the interface. There is a potential to leverage these chemical interactions on TiN from a materials design perspective as well, for example, engineering oxygen and nitrogen vacancies in superlattice structures.

CRediT Authorship Contribution Statement

Xiaoman Zhang: Methodology, Data Collection and Curation, Formal analysis, Investigation, Writing – Original Draft, Writing – Review & Editing.

W.J. Meng: Conceptualization, Data Collection and Curation, Validation, Investigation, Resources, Writing – Original Draft, Writing

This journal is © The Royal Society of Chemistry 20xx

- Review & Editing, Supervision, Project administration, Funding acquisition.

Andrew C. Meng: Conceptualization, Methodology, Data Collection and Curation, Formal analysis, Investigation, Writing – Original Draft, Writing - Review & Editing.

Conflicts of Interest

The authors declare no competing interests in the matter of this manuscript.

Acknowledgements

XZ and WJM acknowledge partial project support from NSF EPSCoR program under awards OIA-1541079 and OIA-1946231 and use of experimental facilities at the LSU Shared Instrumentation Facility (SIF), a part of the Louisiana Core User Facilities (CUF). Technical assistance from staff members from ThermoFisher Nanoport (Hillsboro, OR) is acknowledged with thanks.

References

1. T. Szyjka, L. Baumgarten, T. Mittmann, Y. Matveyev, C. Schlueter, T. Mikolajick, U. Schroeder and M. Müller, *ACS Appl. Electron. Mater.*, 2020, **2**, 3152-3159.
2. T. Nishimura, L. Xu, S. Shibayama, T. Yajima, S. Migita and A. Toriumi, *Jpn. J. Appl. Phys.*, 2016, **55**, 08PB01.
3. P. D. Lomenzo, P. Zhao, Q. Takmeel, S. Moghaddam, T. Nishida, M. Nelson, C. M. Fancher, E. D. Grimley, X. Sang, J. M. LeBeau and J. L. Jones, *J. Vac. Sci. Technol. B*, 2014, **32**, 03D123.
4. D. H. Triyoso, P. J. Tobin, B. E. W. Jr., R. Gregory and X. D. Wang, *Appl. Phys. Lett.*, 2006, **89**, 132903.
5. S. Petzold, A. Zintler, R. Eilhardt, E. Piros, N. Kaiser, S. U. Sharath, T. Vogel, M. Major, K. P. McKenna, L. Molina-Luna and L. Alff, *Adv. Electron. Mater.*, 2019, **5**, 1900484.
6. H. J. Lee, J. H. Hwang, J.-Y. Park and S. W. Lee, *ACS Appl. Electron. Mater.*, 2021, **3**, 999-1005.
7. R. I. Hegde, P. J. Tobin, K. G. Reid, B. Maiti and S. A. Ajuria, *Appl. Phys. Lett.*, 1995, **66**, 2882-2884.
8. H. Shang, K.-L. Lee, P. Kozlowski, C. D. Emic, I. Babich, E. Sikorski, I. Meikei, H. S. P. Wong, K. Guarini and W. Haensch, *IEEE Electron Device Lett.*, 2004, **25**, 135-137.
9. J. Thangala, Z. Chen, A. Chin, C.-Z. Ning and M. K. Sunkara, *Cryst. Growth Des.*, 2009, **9**, 3177-3182.
10. X. Wang, J. Jian, H. Wang, J. Liu, Y. Pachaury, P. Lu, B. X. Rutherford, X. Gao, X. Xu, A. El-Azab, X. Zhang and H. Wang, *Small*, 2021, **17**, 2007222.
11. D. Zhang, H. Cui, C. Zhu, K. Lv, H. Zhang, X. Liu and J. Qiu, *ACS appl. Mater. Interfaces*, 2021, **13**, 1253-1260.
12. D. Walczyk, T. Bertaud, M. Sowinska, M. Lukosius, M. A. Schubert, A. Fox, D. Wolansky, A. Scheit, M. Fraschke, G. Schoof, C. Wolf, R. Kraemer, B. Tillack, R. Korolevych, V. Stikanov, C. Wenger, T. Schroeder and C. Walczyk, 2012.
13. P. Calka, E. Martinez, V. Delaye, D. Lafond, G. Audoit, D. Mariolle, N. Chevalier, H. Grampeix, C. Cagli, V. Jousseaume and C. Guedj, *Nanotechnology*, 2013, **24**, 085706.
14. J.-H. Chang, C.-G. Zheng, H.-H. Chen, P.-T. Chen, C.-B. Liu, K.-Y. Huang, H.-H. Hsu, C.-H. Cheng, W.-C. Chou and S.-T. Han, *Thin Solid Films*, 2022, **753**, 139274.
15. S. Starschich, S. Menzel and U. Böttger, *Appl. Phys. Lett.*, 2016, **108**.
16. R. He, H. Wu, S. Liu, H. Liu and Z. Zhong, *Phys. Rev. B*, 2021, **104**, L180102.
17. Z. Yong, K.-M. Persson, M. Saketh Ram, G. D'Acunto, Y. Liu, S. Benter, J. Pan, Z. Li, M. Borg, A. Mikkelsen, L.-E. Wernersson and R. Timm, *Appl. Surf. Sci.*, 2021, **551**, 149386.
18. H. Qiao, C. Wang, W. S. Choi, M. H. Park and Y. Kim, *Mater. Sci. Eng. R Rep.*, 2021, **145**, 100622.
19. J. Lee, J. Park, S. Jung and H. Hwang, 2011.
20. L. Hultman, S. A. Barnett, J. E. Sundgren and J. E. Greene, *J. Cryst. Growth*, 1988, **92**, 639-656.
21. N. Biunno, J. Narayan, A. R. Srivatsa and O. W. Holland, *Appl. Phys. Lett.*, 1989, **55**, 405-407.
22. X. Zhang, R. Namakian, A. C. Meng, D. Moldovan and W. J. Meng, *Mater. Sci. Eng. A*, 2022, **855**, 143889.
23. X. Zhang, S. Shao, A. S. M. Miraz, C. D. Wick, B. R. Ramachandran and W. J. Meng, *Materialia*, 2020, **12**, 100748.
24. C. Su and J. Zhang, *Comput. Mater. Sci.*, 2021, **189**, 110257.
25. D. Chen, X. L. Ma, Y. M. Wang and L. Chen, *Phys. Rev. B*, 2004, **69**, 155401.
26. T. Li, T. Liu, H. Wei, S. Hussain, B. Miao, W. Zeng, X. Peng and F. Pan, *Comput. Mater. Sci.*, 2015, **105**, 83-89.
27. L. Hultman, J. E. Sundgren and D. Hesse, *J. Mater. Res.*, 1989, **4**, 1266-1271.
28. L. Hultman, D. Hesse and W. A. Chiou, *J. Mater. Res.*, 1991, **6**, 1744-1749.
29. L.-L. Wei and L. Chang, *Mater. Lett.*, 2018, **213**, 227-230.
30. S. Miyagawa, K. Saitoh, H. Niwa, M. Ikeyama, G. Massouras and Y. Miyagawa, *J. Appl. Phys.*, 1992, **72**, 5663-5667.
31. L. Braic, N. Vasilantonakis, A. Mihai, I. J. Villar Garcia, S. Fearn, B. Zou, N. M. Alford, B. Doiron, R. F. Oulton, S. A. Maier, A. V. Zayats and P. K. Petrov, *ACS Appl. Mater. Interfaces*, 2017, **9**, 29857-29862.
32. J.-M. Chappé, N. Martin, J. Lintymer, F. Sthal, G. Terwagne and J. Takadoum, *Appl. Surf. Sci.*, 2007, **253**, 5312-5316.
33. J. Huang, D. Zhang and H. Wang, *Mater. Today Phys.*, 2021, **16**, 100316.
34. W.-C. Chen, C.-Y. Peng and L. Chang, *Nanoscale Res. Lett.*, 2014, **9**, 551.
35. L.-L. Wei, T.-C. Yen, H. Do and L. Chang, *Thin Solid Films*, 2016, **618**, 8-12.
36. L. Hultman, J. E. Sundgren and J. E. Greene, *J. Appl. Phys.*, 1989, **66**, 536-544.
37. M. Xue, R. Islam, A. C. Meng, Z. Lyu, C.-Y. Lu, C. Tae, M. R. Braun, K. Zang, P. C. McIntyre, T. I. Kamins, K. C. Saraswat and J. S. Harris, *ACS Appl. Mater. Interfaces*, 2017, **9**, 41863-41870.
38. G. K. Reeves and H. B. Harrison, *IEEE Electron Device Lett.*, 1982, **3**, 111-113.
39. S. Kirchhoff, *Ann. Phys.*, 1845, **140**, 497-514.
40. H. v. Seefeld, N. W. Cheung, M. Maenpaa and M. A. Nicolet, *IEEE Trans. Electron Devices*, 1980, **27**, 873-876.
41. N. K. Ponon, D. J. R. Appleby, E. Arac, P. J. King, S. Ganti, K. S. K. Kwa and A. O'Neill, *Thin Solid Films*, 2015, **578**, 31-37.
42. L. Hultman, L. R. Wallenberg, M. Shinn and S. A. Barnett, *J. Vac. Sci. Technol. A*, 1992, **10**, 1618-1624.

43. C. H. Lei, A. A. Rockett, I. M. Robertson, N. Papathanasiou and S. Siebentritt, *J. Appl. Phys.*, 2006, **100**.
44. X. Meng, A. Ueki, H. Tatsuoka and H. Itahara, *Chem. Eur. J.*, 2017, **23**, 3098-3106.
45. Y. Nakanishi, A. Miyake, H. Tatsuoka, H. Kominami, H. Kuwabara and Y. Hatanaka, *Appl. Surf. Sci.*, 2005, **244**, 359-364.
46. J. H. Han and J. H. Bang, *J. Mater. Chem. A*, 2014, **2**, 10568-10576.
47. K.-C. Han, G.-Q. Lin, C. Dong, K.-P. Tai and X. Jiang, *Acta Metall. Sin.-Engl.*, 2017, **30**, 1100-1108.
48. K. Tang, A. C. Meng, F. Hui, Y. Shi, T. Petach, C. Hitzman, A. L. Koh, D. Goldhaber-Gordon, M. Lanza and P. C. McIntyre, *Nano Lett.*, 2017, **17**, 4390-4399.

This journal is © The Royal Society of Chemistry 20xx